scientific reports

Check for updates

OPEN

# Prognosis prediction via histological evaluation of cellular heterogeneity in glioblastoma

Mari Kirishima[1,7], Seiya Yokoyama[1,7], Toshiaki Akahane[1,2], Nayuta Higa[3], Hiroyuki Uchida[3], Hajime Yonezawa[3], Kei Matsuo[1], Junkoh Yamamoto[4], Koji Yoshimoto[5], Ryosuke Hanaya[3]✉ & Akihide Tanimoto[1,2,6]✉

**Glioblastomas (GBMs) are the most aggressive types of central nervous system tumors. Although certain genomic alterations have been identified as prognostic biomarkers of GBMs, the histomorphological features that predict their prognosis remain elusive. In this study, following an integrative diagnosis of 227 GBMs based on the 2021 World Health Organization classification system, the cases were histologically fractionated by cellular variations and abundance to evaluate the relationship between cellular heterogeneity and prognosis in combination with *O*-6-methylguanine-DNA methyltransferase gene promoter methylation (m*MGMTp*) status. GBMs comprised four major cell types: astrocytic, pleomorphic, gemistocytic, and rhabdoid cells. *t*-distributed stochastic neighbor embedding analysis using the histological abundance of heterogeneous cell types identified two distinct groups with significantly different prognoses. In individual cell component analysis, the abundance of gemistocytes showed a significantly favorable prognosis but confounding to m*MGMTp* status. Conversely, the abundance of epithelioid cells was correlated with the unfavorable prognosis. Linear model analysis showed the favorable prognostic utility of quantifying gemistocytic and epithelioid cells, independent of m*MGMTp*. The evaluation of GBM cell histomorphological heterogeneity is more effective for prognosis prediction in combination with m*MGMTp* analysis, indicating that histomorphological analysis is a practical and useful prognostication tool in an integrative diagnosis of GBMs.**

**Keywords** Glioblastoma, Cell heterogeneity, Gemistocyte, Prognosis, Methylation of *MGMT* promoter

Glioblastomas (GBMs) are malignant glial tumors of the central nervous system (CNS), accounting for 15% of all CNS gliomas and primarily affecting older individuals[1]. The current standard treatment for GB involves surgical resection followed by radiotherapy and temozolomide (TMZ) chemotherapy. Despite these intensive and multimodal therapies, the prognosis is poor, with a median survival of approximately 1.5 years post-diagnosis and a five-year survival rate of less than 5%[1–3].

With the increased use of next-generation sequencing (NGS) for genomic profiling of gliomas, our understanding of GBMs has advanced. Genomic alternations such as *EGFR*, *PDGFRA*, and *CDKN2A*, as well as methylation of the *O*-6-methylguanine-DNA methyltransferase gene promoter (m*MGMTp*), have become hallmarks of prognosis prediction [4–9]. GBM cells exhibit morphological diversity, including fibrillary, adenoid (epithelioid), gemistocytic, granular, oligodendroglioma (ODG)-like, primitive neuronal differentiation (PND)-like (formerly primitive neuroectodermal tumor-like), giant, and small cells [10,11]. Among these variants of GBM, those predominantly displaying epithelioid and rhabdoid features have been suggested to have an unfavorable prognosis [12–14]. However, the prognosis of patients with variant GBMs exhibiting predominantly small, giant,

[1]Department of Pathology, Kagoshima University Graduate School of Medical and Dental Sciences, 8-35-1 Sakuragaoka, Kagoshima 890-8544, Japan. [2]Center for Human Genome and Gene Analysis, Kagoshima University Hospital, 8-35-1 Sakuragaoka, Kagoshima 890-8544, Japan. [3]Department of Neurosurgery, Kagoshima University Graduate School of Medical and Dental Sciences, 8-35-1 Sakuragaoka, Kagoshima 890-8544, Japan. [4]Department of Neurosurgery, University of Occupational and Environmental Health, Yahatanishi-Ku, Kitakyushu 807-8555, Japan. [5]Department of Neurosurgery, Graduate School of Medical Sciences, Kyushu University, 3-1-1 Maidashi, Higashi-Ku, Fukuoka 812-8582, Japan. [6]Center for the Research of Advanced Diagnosis and Therapy of Cancer, Kagoshima University Graduate School of Medical and Dental Sciences, Kagoshima, Japan. [7]Mari Kirishima and Seiya Yokoyama contributed equally to this study. ✉email: hanaya@m2.kufm.kagoshima-u.ac.jp; akit09@m3.kufm.kagoshima-u.ac.jp

PND-like, and ODG-like components remains controversial or comparable to GBM not otherwise specified (GB-NOS) [13,15,16]. Additionally, the presence of intratumoral thrombi has been correlated with a poor prognosis [17]. However, the occurrence of thrombus in GBM cases showing specific cellular features has not been documented.

Despite the heterogeneous cellular composition of GBMs, few studies have assessed GBM prognosis based on their cellular heterogeneity. Furthermore, since the introduction of the latest 2021 World Health Organization (WHO) classification [10], some cases previously diagnosed as GBM based on the histological presence of microvascular proliferation and palisading necrosis have been reclassified as astrocytoma grade 4 if they harbor pathogenic *IDH* mutations [18,19]. Therefore, a comprehensive review of GBM histopathology is essential to delineate the distinctive histomorphological features of GBM cells and re-evaluate the relationship between cellular morphology and prognosis. Consequently, establishing simple, practical, and useful histomorphological indicators for prognosis is crucial for refining therapeutic strategies and optimizing patient management.

In this study, we aimed to construct a prediction model for GBM prognosis based on the evaluation of the histological abundance of heterogeneous GBM cellular constituents, regardless of the diagnosis of GBM variants or GBM-NOS. We sought to identify GB cellular constituents predictive of prognosis, irrespective of m*MGMTp* status, a well-established prognostic marker of GBM that regulates TMZ response via *MGMT* expression [20–22]. We analyzed 227 cases of GBs confirmed by pathological and genomic integrative examinations using a glioma-targeted NGS panel in accordance with the 2021 WHO classification [10]. Additionally, the m*MGMTp* status was analyzed using methylation-specific PCR (MSP). The association of the histological abundance of heterogeneous GBM cellular constituents with m*MGMTp* status and prognosis was investigated using *t*-distributed stochastic neighbor embedding (*t*-SNE).

## Results

### Clinical information and integrative diagnosis

The clinical information of the patients with GBM (n = 227) is summarized in Supplementary Table S1. Of these 227 patients, 106 were treated by almost total surgical excision of tumors (≥ 90% excision of total tumor volume). Additionally, 214 and 210 patients were treated with chemotherapy and radiotherapy, respectively. Histological findings (presence or absence of necrosis/microvascular proliferation) and genomic alterations necessary for integrative diagnosis based on the 2021 WHO classification are summarized in Fig. 1.

### Representative histology of each cellular component

The representative morphologies of heterogeneous cellular constituents assessed using HE staining are shown in Figs. 2A–2K. Histological observations revealed two major cellular components; pleomorphic and astrocytic (Fig. 2L). Among the 227 patients, pleomorphic cells accounted for 33% of the tumor area, followed by 29.1% and 10.4% for astrocytic and gemistocytic cells, respectively (Fig. 3A). Identification of cellular constituents with over 10% area revealed that 15% of cases had only astrocytic cells (34/227), 11.5% had only pleomorphic cells (26/227), and 52% harbored two cell components, with combinations of pleomorphic + gemistocytic cells in 13.7% (31/227), astrocytic + gemistocytic cells in 9.7% (22/227), and other combinations (28.6%). Other minor cellular components included epithelioid, small, giant, ODG-like, PND-like, and lipidized cells in different combinations (Fig. 3B).

### Methylation of *MGMTp* (m*MGMTp*) status

In the analyzable 224 cases, the hypomethylation value of *MGMTp* was 73 ± 31. Categorization of m*MGMTp* status based on low methylation (hypomethylation values ≥ 84.63 as low-m*MGMTp*) and high methylation (hypomethylation values < 84.63 as high-m*MGMTp*) revealed that high-m*MGMTp* cases (n = 101, blue line) had a significantly favorable prognosis compared with low-m*MGMTp* cases (n = 123, red line) [Fig. 4; hazard ratio (HR), 0.415; 95% confidence interval (CI), 0.287–0.601; $p < 0.001$].

### Gene alterations and prognosis

Analysis of the relationships between gene alterations and prognosis revealed that *PDGFRA* mutations (n = 16) and amplification (n = 37) were associated with an unfavorable prognosis. In contrast, *PTEN* loss (n = 92) was associated with a favorable prognosis. *BRAF*, *EGFR*, *PTEN*, and *TERTp* promoter mutations and *EGFR* amplification showed no prognostic significance (Supplementary Table S2).

### *Beta* diversity analysis of cell morphology and prognosis

To evaluate the association between cellular heterogeneity and prognosis, beta diversity analysis was performed using *t*-SNE (Fig. 5). The arrows on t-SNE plot indicate tendencies or directions of correlation, but they do not imply definitive clustering or a direct link to individual patient outcomes based solely on cell type. When two isolated areas (1 and 2) were set in *t*-SNE, astrocytic, rhabdoid, small, and giant cell components were directed toward area 1, whereas gemistocytic, spindle, and pleomorphic cells were directed towards area 2 (Fig. 5A). The prognosis of area 2 patients (n = 91) was found to be significantly better than that of area 1 patients (n = 136) [HR, 0.511; 95% CI, 0.350–0.747; $p < 0.001$; Fig. 5B]. In t-SNE analysis, the consistency of the results across various random seeds was confirmed, ensuring the reproducibility of our findings.

### Predominant cell type and prognosis

Thresholds were set for the histological abundance of each cell type to evaluate the relationship between the predominant cellular type and prognosis (Table 1). Among the four major cellular components, gemistocytic cells were identified in 89 cases. Of these cases, 60 exceeded the threshold of 20% and were significantly correlated with a favorable prognosis (HR, 0.65; 95% CI, 0.43–0.98; $p = 0.038$). Nevertheless, the prognosis

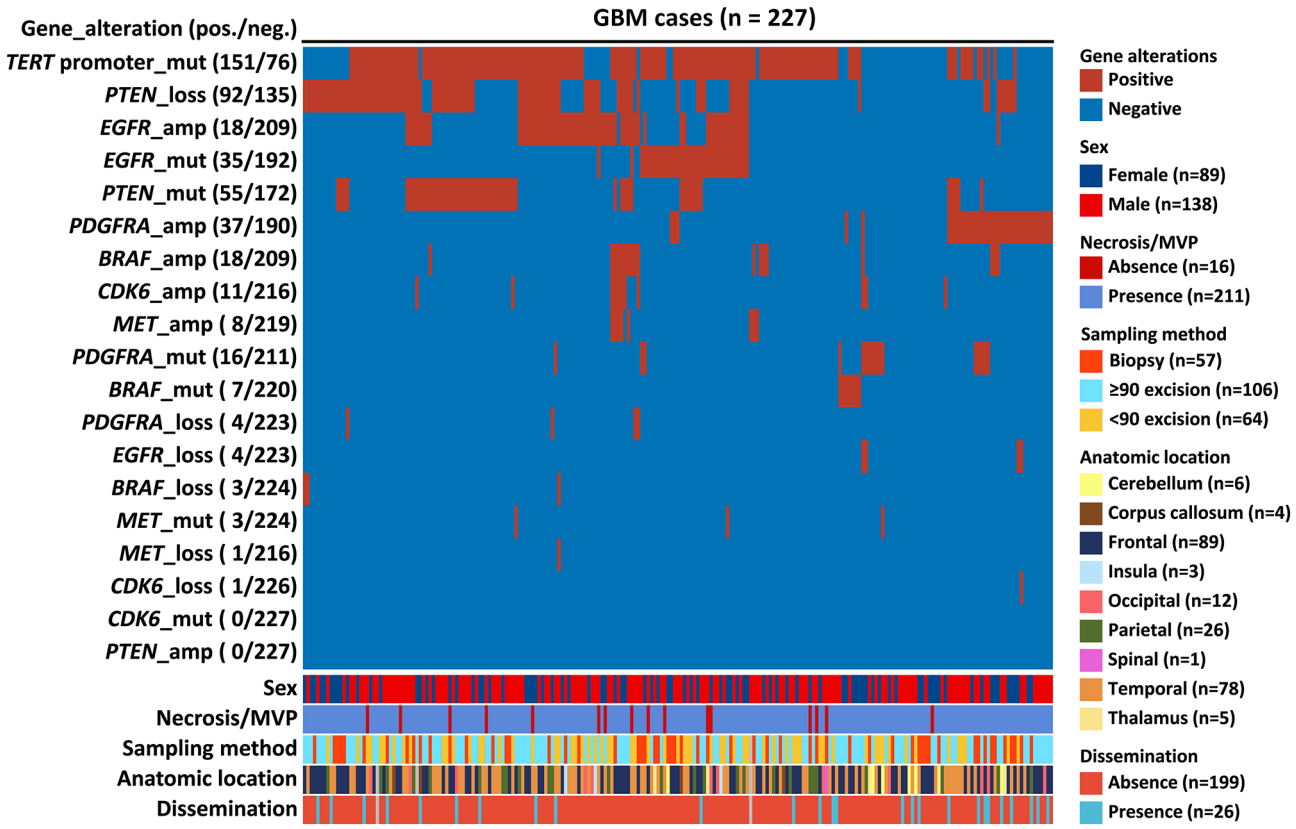


**Fig. 1**. Graphical presentation of gene alterations and histology in GBM cases. The map shows gene alterations, including mutations, amplification, and loss, in the upper panel, necessary for the genomic definition of the 2021 WHO classification. Histology (presence or absence of necrosis/MVP and intrahecal dissemination), tissue sampling methods, and anatomic localization are presented in the lower panel. The tissue sampling methods are classified as biopsy and resection (≥ or < 90% excision of total tumor volume). The cases with presence of necrosis/MVP correspond to histological GBM, and those with absence of necrosis/MVP correspond to molecular GBM. GBM, glioblastoma; MVP, microvascular proliferation

was confounded by several factors, including age, Karnofsky performance status (KPS), chemo/radiotherapy, medullary dissemination, mutations in five genes (*BRAF*, *PDGFRA*, *EGFR*, *PTEN*, and *TERT*p), and m*MGMTp* status. Cases with three major cellular components, including astrocytic, pleomorphic, and rhabdoid cells showed no significant association with prognosis. Conversely, the presence of minor-type epithelioid cells exceeding a threshold of 30% (five of the six epithelioid cell-positive cases) was significantly correlated with an unfavorable prognosis (HR, 6.944; 95% CI, 2.77–17.54; $p < 0.001$), independent of factors such as age, KPS, chemo/radiotherapy, medullary dissemination, mutations of five genes, and m*MGMTp* status.

## Morphological linear *indicator* model for prognosis and *MGMTp* methylation

To construct a screening morphological index that could predict a favorable prognosis, we performed a category-weighting analysis using the abundance of gemistocytic and epithelioid cellular components. A combined morphologic index$^{gemi\text{-}4xepith}$ calculated using a simple and linear formula: [% area of gemistocytic cells minus 4 × % area of epithelioid cells] was identified as the most significant and non-confounding prognostic marker. Patients characterized by ≥ 20% of the index (high-index$^{gemi\text{-}4xepith}$; n = 59) had a significantly more favorable prognosis than those with a value < 20% (low-index$^{gemi\text{-}4xepith}$; n = 168) (HR, 0.625; 95% CI, 0.413–0.946; $p = 0.025$; Fig. 6A). However, no difference was observed between the low- and high-index$^{gemi\text{-}4xepith}$ groups concerning the m*MGMTp* status (Wilcoxon test, $p = 0.361$, delta = 0.08 [-0.09–0.24]). Univariate and multivariate regression analyses for prognosis revealed that the index$^{gemi\text{-}4xepith}$ remained non-confounding based on age, the presence of medullary dissemination, chemotherapy, gene mutations, and m*MGMTp* status (Table 2).

Patients with a high-index$^{gemi\text{-}4xepith}$ and high-m*MGMTp* (n = 24) showed a more favorable prognosis than all other patients (n = 202) (HR, 0.312; 95% CI, 0.162–0.601; $p < 0.001$; Fig. 6B), indicating that the combined m*MGMTp* and morphological index$^{gemi\text{-}4xepith}$ analysis showed a higher effect for favorable prognostication than single m*MGMTp* analysis (Fig. 3) (HRs, 0.312 vs. 0.415, respectively). In contrast, those with a low-index$^{gemi\text{-}4xepith}$ and low-m*MGMTp* (n = 90) had a less favorable prognosis than all others (n = 135) (HR, 2.174; 95% CI; 1.515–3.125; $p < 0.001$; Fig. 6C).

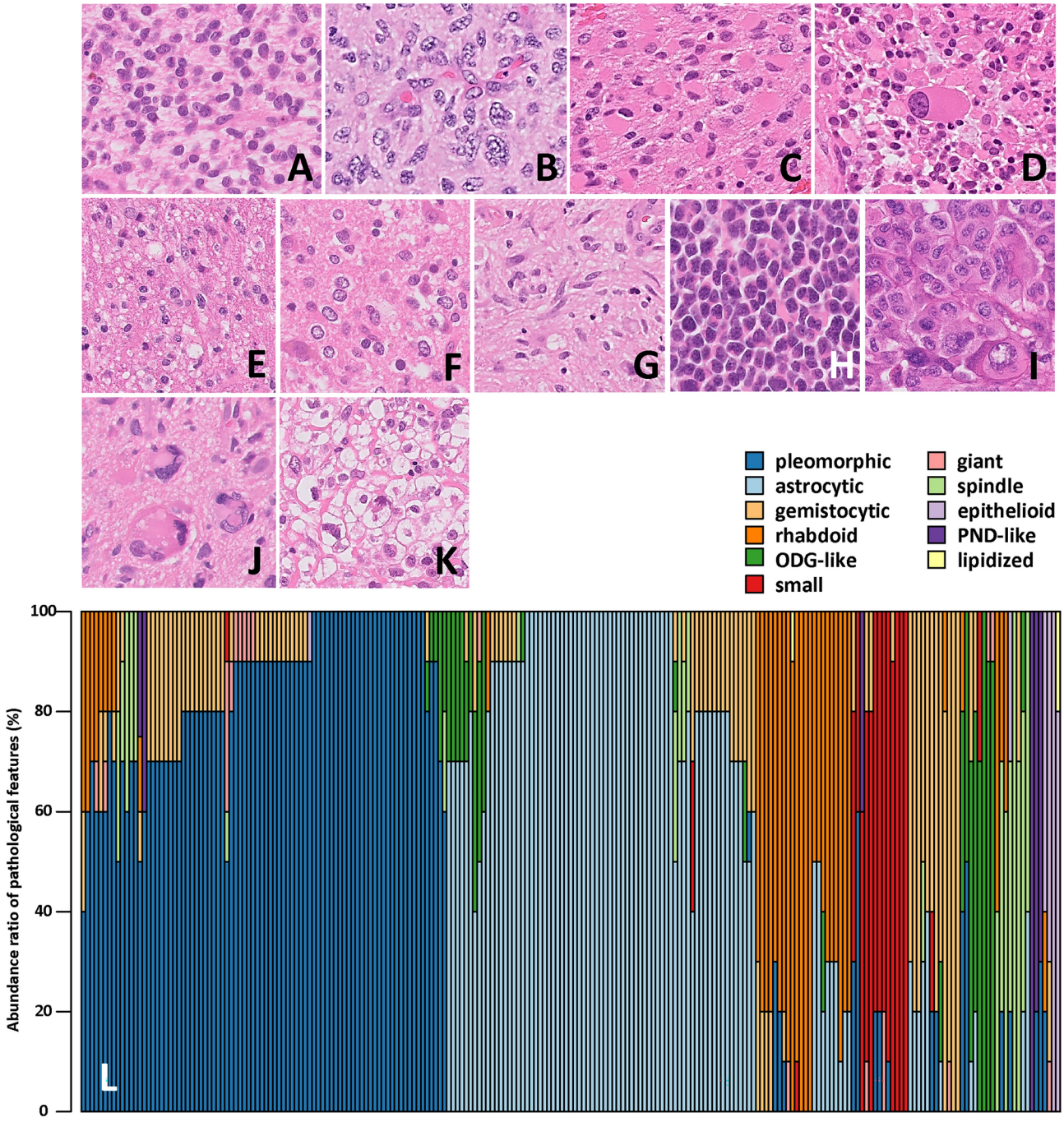


**Fig. 2**. Representative morphology and populations of GBM cellular constituents. **(A) to (K)** The representative features of different tumor cell types shown in HE-stained sections (×400). Astrocytic **(A)** and pleomorphic **(B)** cells are prototypic for glioblastoma. The less frequently detected cell types are as follows: gemistocytic **(C)**, rhabdoid **(D)**, epithelioid **(I)**, and other cell types [**(E)** small; **(F)** ODG-like; **(G)** spindle; **(H)** PND-like; **(J)** giant; **(K)** lipidized]. In panel **D**, a large rhabdoid cell is present within an aggregation of gemistocytic cells. **L)** The vertical axis represents the percentage area of different cellular constituents, and the horizontal axis represents sorted cases. Two major components, astrocytic and pleomorphic cells, are shown in light and dark blue columns, respectively. PND, primitive neuronal differentiation; ODG, oligodendroglioma; HE, hematoxylin and eosin.

## Discussion

The principal achievement of the present study was the evaluation of integrative cellular morphology by histological examination. First, we showed that GBM cases with predominantly gemistocytic components exhibited better prognosis than others, although this was confounded by *mMGMTp* status. Second, the integrated evaluation of the cellular abundance of gemistocytic and epithelioid cells using a linear model

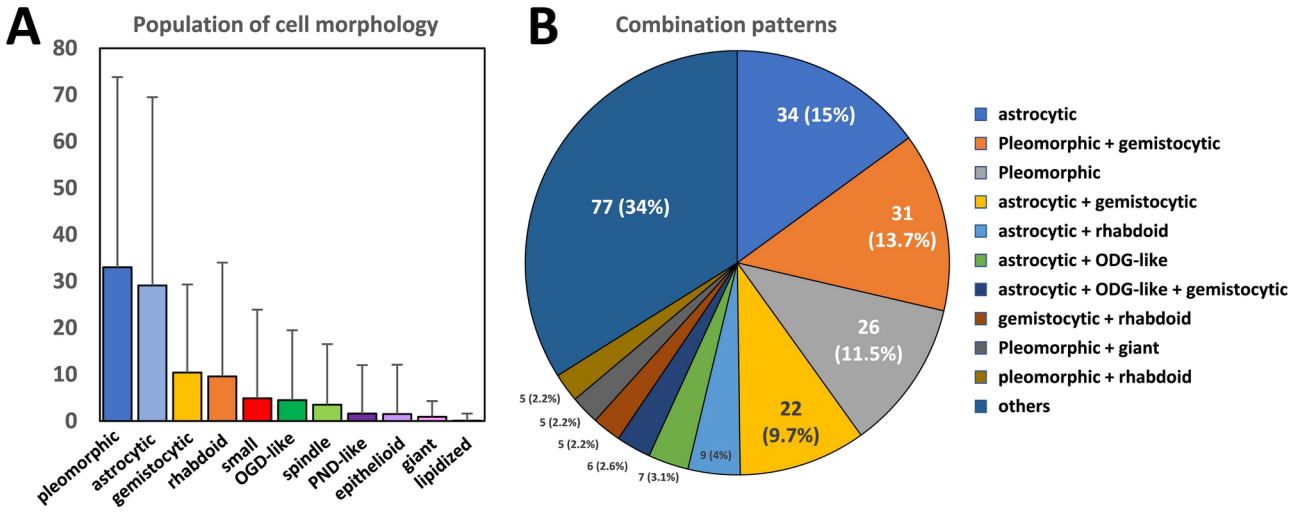


**Fig. 3**. Population and combination patterns of GBM cellular constituents. (**A**) Bar chart showing the population of each cell types. Values are presented as means ± standard deviations. (**B**) Pie chart showing the combination patterns of each cell types. Values are numbers of cases, and percentages of cases are shown in the parentheses.

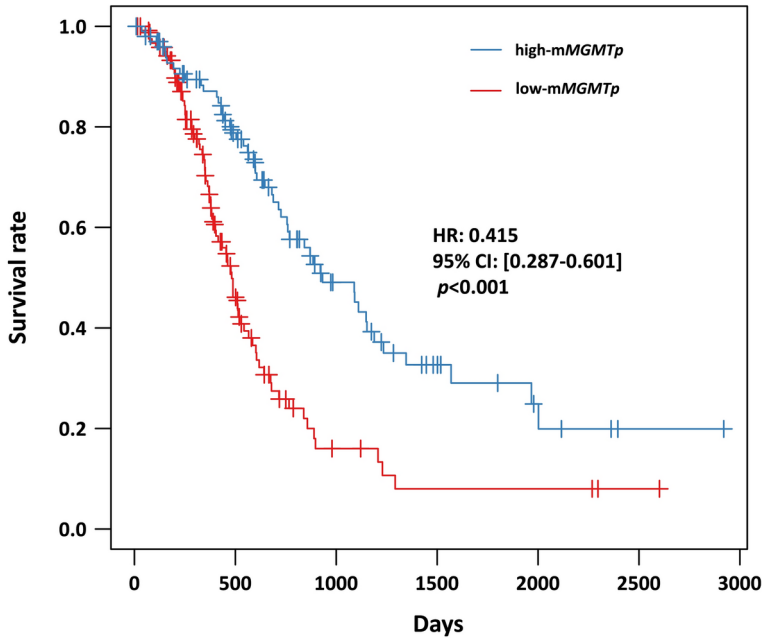


**Fig. 4**. m*MGMTp* status and prognosis. Patients with a high-m*MGMTp* (blue line) showed a more favorable prognosis than those with a low-m*MGMTp* (red line). m*MGMTp* was analyzed in 224 of the 227 cases. *MGMT*, o-6-methylguanine-DNA methyltransferase gene; m*MGMTp*,*MGMT* promoter methylation; HR, hazards ratio; 95% CI, 95% confidence interval

predicted prognosis, independent of *mMGMTp* status and exhibited a synergistic effect on prognostication when combined with *mMGMTp* analysis. The combined analytical approach, which fractionated each GBM case by cellular composition using a common histological examination and PCR-based *mMGMTp* analysis, could be essential and practical for evaluating the relationship between histomorphology and prognosis, as GBMs usually consist of heterogeneous tumor cells [10,11]. Collectively, these findings indicate the successful establishment of an independent histomorphological prognostication method and highlight the importance of histological profiling of heterogeneous cellular constituents in predicting GBM prognosis.

Even though GBMs are characterized by the proliferation of divergent tumor cell constituents[10,11,23–25], few studies have reported a relationship between GBM cellular components and prognosis. Moreover, the association between the presence of gemistocytes and prognosis has been well studied, with several studies indicating that

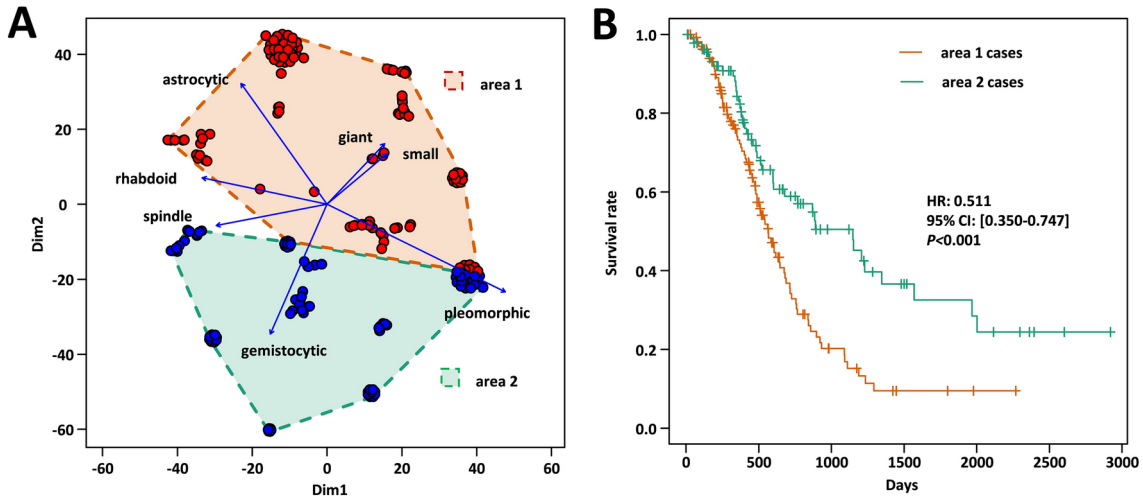


**Fig. 5**. Segmentation of cellular constituents analyzed using *t*-SNE and prognosis. (**A**) Regarding Dim2 on the vertical axis, four arrows representing the astrocytic, rhabdoid, small, and giant cell components are directed toward the positive side (area 1), whereas three arrows representing the gemistocytic, spindle, and pleomorphic cells are directed toward the negative side (area 2). (**B**) Cases clustering in area 2 (green line) had a more favorable prognosis than those clustering in area 1 (orange line). HR, hazards ratio; 95% CI, 95% confidence interval

| Morphology | Cases more than 10% area | Threshold | Number of | | *p* value | HR | 95% IC | Regression analysis | |
|---|---|---|---|---|---|---|---|---|---|
| | | | Cases ≥ threshold | Cases < threshold | | | | Univariate | Multivariate |
| Pleomorphic | 102/227 | 100 | 26 | 201 | 0.158 | 0.627 | 0.33–1.2 | 0.385 | 0.715 |
| Astrocytic | 90/227 | 70 | 63 | 164 | 0.288 | 1.239 | 0.83–1.84 | 0.764 | 0.483 |
| Gemisticytic | 89/227 | 20 | 60 | 167 | 0.038 | 0.65 | 0.43–0.98 | 0.139 | 0.117 |
| Rhabdoid | 38/227 | 90 | 7 | 220 | 0.117 | 2.028 | 0.82–5 | 0.869 | 0.958 |
| ODG-like | 28/227 | 100 | 1 | 226 | < 0.001 | 14.925 | 1.96–111.11 | 0.605 | 0.839 |
| Spindle | 21/227 | 100 | 1 | 226 | 0.164 | NA | NA | 0.718 | 0.695 |
| Small | 18/227 | 60 | 11 | 216 | 0.135 | 1.724 | 0.84–3.55 | 0.647 | 0.862 |
| Giant | 17/227 | 30 | 1 | 226 | 0.03 | 6.711 | 0.91–50 | 0.073 | 0.141 |
| Epitheloid | 6/227 | 30 | 5 | 222 | < 0.001 | 6.944 | 2.77–17.54 | < 0.001 | 0.002 |
| PND-like | 6/227 | 25 | 6 | 221 | 0.286 | 1.56 | 0.69–3.55 | 0.602 | 0.414 |
| Lipidized | 2/227 | 10 | 2 | 225 | 0.005 | 6.024 | 1.45–25 | 0.009 | < 0.001 |

**Table 1**. Cell morphology and prognosis. Multivariate regression analysis was performed with clinical information (age, KPS, presence or absence of medullary dissemination, chemotherapy, and radiotherapy), gene mutation data (EGFR, PDGFRA, PTEN, BRAF, TERT promoter), and MGMT methylation data. ODG, oligodendroglioma; PND, primitive neuronal differentiation; NA, not available; HR, hazard ratio; 95% CI, 95% confidence interval.

a high abundance of gemistocytic cells is related to poor prognosis in both low- and high-grade gliomas[26–30]. Gemistocytes, a type of neoplastic cell distinct from reactive astrocytes, are considered an adverse prognostic factor[11,26,29], and grade II astrocytomas containing over 5% gemistocytes are likely to progress rapidly to grade III astrocytomas and grade IV GBM[30]. Additionally, grade II astrocytomas comprising ≥ 20% gemistocytes have been found to have a less favorable prognosis than those comprising ≤ 20% gemistocytes [27]. These studies were performed according to the 2016 WHO classification system and included *IDH* wild-type GBM or cases not elsewhere classified based on the latest 2021 WHO classification. Furthermore, another study including non-negligible cases of *IDH*-mutant astrocytoma showed that the prognosis of GBM cases with ≥ 20% gemistocytes did not differ significantly from those with < 20% gemisotocytes[28]. In contrast, in the present study, we identified the presence of gemistocytes, singly and in combination with other cell types, as histological markers of favorable prognosis of GBMs. Nevertheless, the significance of gemistocytes and other cell types in astrocytomas should be further investigated based on the 2021 WHO classification.

In previous studies, rhabdoid and epithelioid GBMs often harbored *BRAF* V600E mutations, suggesting a close genomic, morphological, and poor prognostic correlation[12–14,24]. Our findings also revealed that some

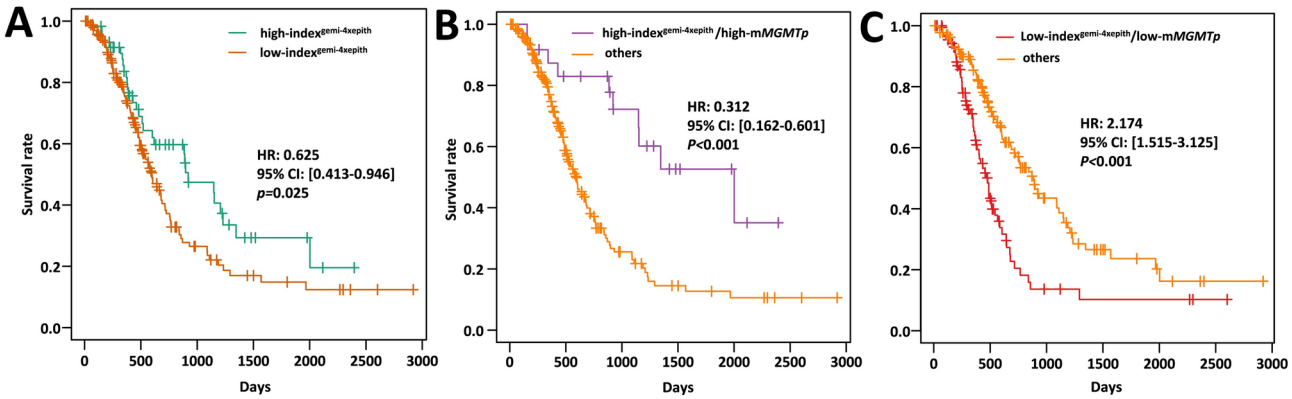


**Fig. 6**. The index$^{gemi\text{-}4xepith}$, m***MGMTp*** status, and prognosis. (**A**) Overall survival curves of low- and high-index$^{gemi\text{-}4xepith}$ groups. Compared with patients in the low-index$^{gemi\text{-}4xepith}$ group (orange line), those in the high-index$^{gemi\text{-}4xepith}$ group (green line) showed a favorable prognosis (**B**) Prognosis of patients with a high-index$^{gemi\text{-}4xepith}$ and high-m*MGMTp* and that of others. Patients with a high-index$^{gemi\text{-}4xepith}$ and high-m*MGMTp* (purple line) showed a more favorable prognosis compared with other patients (orange line). (**C**) Prognosis of patients with a low-index$^{gemi\text{-}4xepith}$ and low-m*MGMTp* and that of others. Patients with a low-index$^{gemi\text{-}4xepith}$ and low-m*MGMTp* (red line) had a less favorable prognosis than patients (orange line). *MGMT*, *O*-6-methylguanine-DNA methyltransferase gene; m*MGMTp*, *MGMT* promoter methylation; HR, hazards ratio; 95% CI, 95% confidence interval.

| | Univariate | | Multivariate | |
|---|---|---|---|---|
| | z | *p* | z | *p* |
| **Index$^{gemi\text{-}4xepith}$** | −4.289 | < 0.001 | −3.818 | < 0.001 |
| **Age** | 2.900 | 0.004 | 3.051 | 0.002 |
| **KPS** | −1.345 | 0.179 | −0.739 | 0.460 |
| **Excision degree** | 2.842 | 0.004 | 1.852 | 0.064 |
| **Dissemination** | 5.797 | < 0.001 | 4.791 | < 0.001 |
| **Chemotherapy** | −7.396 | < 0.001 | −2.720 | 0.007 |
| **Radiotherapy** | −6.211 | − 0.001 | −1.702 | 0.089 |
| ***EGFR*** | 0.018 | 0.985 | 0.601 | 0.548 |
| ***PDGFRA*** | 2.277 | 0.023 | 1.998 | 0.046 |
| ***PTEN*** | -0.225 | 0.822 | −0.490 | 0.624 |
| ***BRAF*** | 0.076 | 0.940 | 1.071 | 0.284 |
| ***TERTp*** | 1.082 | 0.279 | 1.410 | 0.159 |
| **m*MGMTp*** | 4.985 | < 0.001 | 4.846 | < 0.001 |

**Table 2**. Regression analysis of index$^{gemi\text{-}4xepith}$. Number of event = 125. Multivariate regression analysis was performed with clinical information (age, KPS, presence or absence of medullary dissemination, chemotherapy, and radiotherapy), gene mutation data (EGFR, PDGFRA, PTEN, BRAF, TERT promoter), and MGMT methylation data. KPS, Karnofsky performance status; *EGFR*, epidermal growth factor receptor; *PDGFRA*, platelet derived growth factor receptor alpha; *PTEN*, phosphatase, tensin homolog deleted on chromosome10; *BRAF*, v-raf murine sarcoma viral oncogene homolog B; *TERTp*, telomerase reverse transcriptase promoter; m*MGMTp*, methylation of o-6-methylguanine-DNA methyltransferase gene promoter.

patients with predominantly rhabdoid cells (7/38, cases with over 90% rhabdoid cells) harbored a *BRAF* V600E mutation but exhibited no significant prognostic differences compared to other patients. Moreover, we identified some GBM cases with epithelioid cell components (5/6, cases with over 30% epithelioid cells) characterized by the absence of *BRAF* alterations, but showed poor prognosis. This discrepancy may be attributed to the small number of such cases in the present study, although the frequency of rhabdoid and epithelioid variants in GBMs was comparable to that in a previous study[13]. Another possibility is that clear differentiation of rhabdoid and epithelioid cells is often challenging, as the criteria for histological variants of rhabdoid or epithelioid GBM are not always well-defined[23–25]. Some studies have reported immunohistochemical differentiation of these two GBM cell types[24,25]. However, other recent studies, including genetic molecular analyses, did not clearly distinguish these two cellular variants, describing cases as epithelioid GBMs harbored both epithelioid and rhabdoid cells with heterogeneous molecular features[31,32]. In this study, the rhabdoid GBM cells were strictly defined as larger rhabdomyoblast-like cells with a loosely cohesive proliferation to differentiate from smaller

epithelioid cells arranged in an epithelial nest-like proliferation pattern. The differentiation of these two GBM cell types remains controversial even after intensive immunohistochemical and molecular analyses. Therefore, it must be emphasized that the present study did not aim to determine the prognosis of specific GBM variants but to estimate the prognosis of GBMs based on the abundance of heterogeneous cellular constituents.

As GBM and pleomorphic xanthoastrocytoma (PXA) share common histological and genomic profiles, such as the presence of pleomorphic cells, *BRAF* V600E mutations, and telomere reverse transcriptase promoter mutations[33,36], the histopathological differential diagnosis of GBM often includes PXA. These similarities indicate that PXA may share certain characteristics with GBM or even transform into GBM[37,38]. However, differentiating pleomorphic cells in GBM from those in PXA based on morphological examinations alone is often contentious. Moreover, *BRAF* V600E mutations account for only 1% of GBs[39,40], making such cases quite rare. In this study, we detected a *BRAF* V600E mutation in seven of the 227 cases, all of which were in GBMs predominantly comprising rhabdoid cells. Our diagnostic approach was integrative, incorporating genomic profiling while excluding cases with typical clinical and diagnostic imaging features of PXA[41].

Further important notices should be acknowledged in the present study. First, the study sample size is not large enough for high generalizability, although the 227 cases examined might not considered so small for evaluating the histology of GBM cellular constituents and its heterogeneity. Access to open resources of public databases for gliomas would be useful for increasing sample size and obtaining genomic and prognostic information[40–42], especially for the rare GBM variants, but these databases often lack detailed histological information on each cell type necessary for our study. Another future approach for increasing the sample size is employing a multi-center study design, which would further validate and strengthen the generalizability of our findings. Second, the influence of specific genetic alterations on GBM cell morphology and prognosis remains unclear. As astrocytic, gemistocytic, and rhabdoid cells may harbor different genomic backgrounds, the diversity in cell morphology and genomic profiles reflects cancer cell plasticity, resulting in histological transformation and divergent prognosis, which is regulated by the summation of complex genetic, epigenetic, and microenvironmental mechanisms[43,44].

In conclusion, the present study demonstrated the utility of histomorphological analysis in predicting GBM prognosis through the evaluation of cellular heterogeneity. This histological study for GBMs holds significant promise for improving patient outcomes. Future research should continue to explore the potential benefits of integrating histological and genomic approaches in the management of GBMs.

## Methods

### Sample collection

A total of 227 patients who had undergone biopsy or surgery at Kagoshima University Hospital (Kagoshima, Japan) (n = 163), Kyushu University Hospital (Fukuoka, Japan) (n = 47), and University Hospital of Occupational and Environmental Health (Kitakyushu, Japan) (n = 17) between April 2018 and December 2023 were included in this study. GBM tissue samples and patient information were collected from all patients.

### Preparation of histological sections and genomic DNA

Tissues were fixed with phosphate-buffered neutral 10% formalin for 24 h and routinely processed for preparation of formalin-fixed paraffin-embedded tissue (FFPE) sections, which were subsequently used for hematoxylin and eosin (HE) staining, immunohistochemistry (IHC), fluorescent in situ hybridization (FISH), and genomic analysis.

Genomic DNA was extracted from FFPE sections as previously reported and subjected to NGS panel analysis designed for genomic profiling, including assessments of gene mutations, copy number variation, and 1p19q co-deletion[45]. 1p19q co-deletion was also investigated using FISH analysis. MSP was performed on 224 samples (three samples were insufficient for further study) using the extracted genomic DNA, as previously reported[46]. The *MGMT*p hypomethylation index was calculated as the percentage of the intensity of unmethylated bands to the total band intensity using a microchip automated electrophoresis instrument (MCE-202 MultiNA, Shimadzu, Kyoto, Japan) in conjunction with a DNA-1000 kit (Shimadzu).

### Integrative diagnosis of GB based on WHO classification

Representative sections with the largest tumor areas were selected for IHC detection of IDH-1 R132H expression and genomic analysis, as previously described, to determine an integrative diagnosis based on the 2021 WHO classification[10,45,46]. Integrative pathological and molecular diagnoses were confirmed by two board-certified pathologists (MK and AT).

### Morphological analysis

Two board-certified pathologists (MK and AT) performed the semi-quantitative morphological evaluation of the representative HE-stained sections to determine the abundance of heterogeneous types of GBM cellular components according to previously described cellular characteristics [10,11,23,25,47,48]. A representative tumor area was scanned using a light microscope at × 40 magnification, then cell morphology was determined at × 400 magnification according to the definitions described in the section "Definition of cell morphology." Subsequently, the percentage area ratio of each cellular component to total tumor area was estimated in 10% increments across the entire tumor scan as a histological cellular abundance at × 100 magnification. In cases where tumor cells were observed in 20 fields of 100 × magnification, including 10 fields of 100% astrocytic cells, seven fields of 50% astrocytic, 30% pleomorphic, and 20% gemistocytic cells, and three fields of 80% gemistocytic and 20% spindle cells. The area of each cell type was calculated as follows: Astrocytic cell area = [10 (fields) × 100 (%) + 7 (fields) × 50 (%)]/20 (fields) = 67.5%; Pleomorphic cell area = [7 × 30]/20 = 10.5%; Gemistocytic cell

area = [7 × 20 + 3 × 80]/20 = 19%; Spindle cell area = [3 × 20]/20 = 3%. The calculated percentages were rounded to the nearest 10% and the cell component occupying ≥ 10% are was considered significant. Finally, the cell components were evaluated as follows: astrocytic cells (70%), gemistocytic cells (20%), and pleomorphic cells (10%).

## Definition of cell morphology

Astrocytic tumor cells have round nuclei with variable nuclear atypia and fibrillary cytoplasm, characteristic of astrocytic differentiation. Pleomorphic cells are characterized by nuclear enlargement and pleomorphism with an irregular nuclear membrane and prominent nucleoli. Gemistocytic cells have eccentric nuclei with clumped chromatin and glassy non-fibrillary cytoplasm. Epithelioid cells are well-demarcated, loosely cohesive cells with discrete cell borders arranged in a solid pattern or with epithelial cell-like features, resembling metastatic carcinoma. Rhabdoid cells are loosely cohesive with large eccentric or centrally located round nuclei and abundant eosinophilic cytoplasm, resembling rhabdomyoblasts. Spindle cells have elongated spindle nuclei and cytoplasm and exhibit fibroblast-like differentiation. Giant cells are large multinucleated cells with large bizarre lobulated nuclei and abundant cytoplasm. Small cells have small monomorphic round uniform nuclei with sparse cytoplasm. Other minor components of lipidized cells show features of small cytoplasmic vacuoles resembling histiocytic foam cells; PDN-like cells show features of primitive neuronal cells with high nuclear to cytoplasmic ratios and sparse cytoplasm and ODG-like cells have round nuclei with a perinuclear halo, mimicking ODG.

## Statistical analysis

Data were analyzed using R computing environment software version 4.3.0 [49]. The normality of the data distribution was evaluated using the Kolmogorov–Smirnov test. Differences between the two groups were analyzed using the non-parametric Wilcoxon signed-rank test, and the effect size was calculated using Cliff's delta in the "effsize" package. Overall survival (OS) was estimated using the Kaplan–Meier method and compared using log-rank tests. HRs were calculated using a Cox proportional hazards model, and univariate and multivariate regression models for OS were performed using a Cox regression model in the survival package. The analysis of beta diversity to evaluate cellular heterogeneity was performed by *t*-SNE using the "stats" and "Rtsne" packages. The random seed was fixed using the set.seed function. All threshold values were calculated as the most effective prognostic values. Statistical significance was set at $p < 0.05$.

## Data Availability

The datasets generated or analyzed during the current study are not publicly available due to privacy/ethical restrictions but are available from the corresponding author on reasonable request.

Received: 16 July 2024; Accepted: 16 October 2024
Published online: 23 October 2024

## References

1. Grochans, S. et al. *Epidemiology of glioblastoma multiforme-literature review. Cancers (Basel)* **14**, 2412 (2022).
2. Louis, D. N. et al. The 2016 World Health Organization classification of tumors of the central nervous system: a summary. *Acta Neuropathol.* **13**, 803–820 (2016).
3. Tykocki, T., Eltayeb, M. Ten-year survival in glioblastoma. a systematic review. *J Clin Neurosci.* **54**, 7–13 (2018).
4. Alnahhas, I. *et al.* Prognostic implications of epidermal and platelet-derived growth factor receptor alterations in 2 cohorts of IDHwt glioblastoma. *Neurooncol. Adv.* **3**, vdab127 (2021).
5. Dundar, B. et al. Molecular characterization and survival analysis of a cohort of glioblastoma. *IDH-wildtype. Pathol. Res. Pract.* **257**, 155272 (2024).
6. Khabibov, M. et al. Signaling pathways and therapeutic approaches in glioblastoma multiforme (review). *Int. J. Oncol.* **60**, 69 (2022).
7. Makino, R. *et al.* Alterations in *EGFR* and *PDGFRA* are associated with the localization of contrast-enhancing lesions in glioblastoma. *Neurooncol. Adv.* **5**, vdad110 (2023).
8. Sasmita, A. O., Wong, Y. P. & Ling, A. P. K. Biomarkers and therapeutic advances in glioblastoma multiforme. *Asia Pac. J. Clin. Oncol.* **14**, 40–51 (2018).
9. Siegal, T. Clinical relevance of prognostic and predictive molecular markers in gliomas. *Adv. Tech. Stand. Neurosurg.* **43**, 91–108 (2016).
10. Brat, D. J. *et al.* Gliomas, glioneuronal tumours, and neuronal tumours in *WHO Classification of Tumours: Central nervous system tumours*, *5th edn* (ed. WHO Classification of Tumours Editorial Board) 15–188 (International Agency for Research on Cancer, 2021).
11. Miller, C. R. & Perry, A. Glioblastoma. *Arch. Pathol. Lab. Med.* **131**, 397–406 (2007).
12. Korshunov, A. et al. Epithelioid glioblastomas stratify into established diagnostic subsets upon integrated molecular analysis. *Brain Pathol.* **28**, 656–662 (2018).
13. Mallick, S., Benson, R., Venkatesulu, B., Melgandi, W. & Rath, G. K. Systematic review and individual patient data analysis of uncommon variants of glioblastoma: an analysis of 196 cases. *Neurol. India* **70**, 2086–2092 (2022).
14. Sun, K. et al. Clinicopathological characteristics and treatment outcomes of epithelioid glioblastoma. *Neurosurg. Rev.* **44**, 3335–3348 (2021).
15. Kozak, K. R. & Moody, J. S. Giant cell glioblastoma: a glioblastoma subtype with distinct epidemiology and superior prognosis. *Neuro. Oncol.* **11**, 833–841 (2009).
16. Perry, A., Aldape, K. D., George, D. H. & Burger, P. C. Small cell astrocytoma: an aggressive variant that is clinicopathologically and genetically distinct from anaplastic oligodendroglioma. *Cancer* **101**, 2318–2326 (2004).
17. Furuta, T. *et al.* Intratumoral thrombosis as a histological biomarker for predicting epidermal growth factor receptor alteration and poor prognosis in patients with glioblastomas. *J. Neurooncol.* **164**, 633–634 (3023).
18. Keric, N. et al. Treatment outcome of IDH1/2 wildtype CNS WHO grade 4 glioma histologically diagnosed as WHO grade II or III astrocytomas. *J. Neurooncol.* **167**, 133–144 (2024).

19. Louis, D., von Deimling, A., Cavenee, W. K. Diffuse astrocytic and oligodendroglial tumours in *World Health Organization classification of tumours of the central nervous system, revised 4th edn.* (eds. Lous, D. N., Ohgaki, H., Wiestler, O., Cavenee, W. K.) 15–78 (International Agency for Research on Cancer, 2016).
20. Hegi, M. E. et al. MGMT gene silencing and benefit from temozolomide in glioblastoma. *N. Engl. J. Med.* **352**, 997–1003 (2005).
21. Malmstrom, A. et al. Temozolomide versus standard 6-week radiotherapy versus hypofractionated radiotherapy in patients older than 60 years with glioblastoma: the Nordic randomised, phase 3 trial. *Lancet Oncol.* **13**, 916–926 (2012).
22. Wick, W. et al. Temozolomide chemotherapy alone versus radiotherapy alone for malignant astrocytoma in the elderly: the NOA-08 randomised, phase 3 trial. *Lancet Oncol.* **13**, 707–715 (2012).
23. Ahrendsen, J. T., Freund, R. S., Hsu, N., Bryke, C. & Varma, H. Cytogenetic and molecular characterization of IDH-wildtype glioblastomas and grade 4 IDH-mutant astrocytomas with unusual histology. *J. Neuropathol. Exp. Neurol.* **81**, 996–1001 (2022).
24. Kleinschmidt-DeMasters, B. K. et al. Epithelioid versus rhabdoid glioblastomas are distinguished by monosomy 22 and immunohistochemical expression of INI-1 but not claudin 6. *Am. J. Surg. Pathol.* **34**, 341–354 (2010).
25. Sugimoto, K. et al. Epithelioid/rhabdoid glioblastoma: a highly aggressive subtype of glioblastoma. *Brain Tumor Pathol.* **33**, 137–146 (2016).
26. Kros, J. M., Waarsenburg, N., Hayes, D. P., Hop, W. C. & van Dekken, H. Cytogenetic analysis of gemistocytic cells in gliomas. *J. Neuropathol. Exp. Neurol.* **59**, 679–686 (2000).
27. Krouwer, H. G., Davis, R. L., Silver, P. & Prados, M. Gemistocytic astrocytomas: a reappraisal. *J. Neurosurg.* **74**, 399–406 (1991).
28. Laviv, Y. et al. Gemistocytes in newly diagnosed glioblastoma multiforme: clinical significance and practical implications in the modern era. *J. Clin. Neurosci.* **88**, 120–127 (2021).
29. Reis, R. M., Hara, A., Kleihues, P. & Ohgaki, H. Genetic evidence of the neoplastic nature of gemistocytes in astrocytomas. *Acta Neuropathol.* **102**, 422–425 (2001).
30. Watanabe, K., Tachibana, O., Yonekawa, Y., Kleihues, P. & Ohgaki, H. Role of gemistocytes in astrocytoma progression. *Lab. Invest.* **76**, 277–284 (1997).
31. Zeng, Y. et al. Clinicopathological, immunohistochemical and molecular genetic study on epithelioid glioblastoma: a series of fifteen cases with literature review. *Onco. Targets Ther.* **13**, 3943–3952 (2020).
32. Pan, R. et al. Epithelioid glioblastoma exhibits a heterogeneous molecular feature: a targeted next-generation sequencing study. *Front. Oncol.* **12**, 980059 (2022).
33. Ebrahimi, A. et al. Pleomorphic xanthoastrocytoma is a heterogeneous entity with pTERT mutations prognosticating shorter survival. *Acta Neuropathol. Commun.* **10**, 5 (2022).
34. Furuta, T. et al. Clinicopathological and genetic association between epithelioid glioblastoma and pleomorphic xanthoastrocytoma. *Neuropathology* **38**, 218–327 (2018).
35. Lin, Z. et al. Pleomorphic xanthoastrocytoma, anaplastic pleomorphic xanthoastrocytoma, and epithelioid glioblastoma: Case series with clinical characteristics, molecular features and progression relationship. *Clin. Neurol. Neurosurg.* **221**, 107379 (2022).
36. Mahajan, S. et al. The evolution of pleomorphic xanthoastrocytoma: from genesis to molecular alterations and mimics. *Lab. Invest.* **102**, 670–681 (2022).
37. Behling, F. et al. Frequency of BRAF V600E mutations in 969 central nervous system neoplasms. *Diagn. Pathol.* **11**, 55 (2016).
38. Ghanem, P. *et al*. Druggable genomic landscapes of high-grade gliomas. *Front. Med. (Lausanne)* **10**, 1254955 (2023).
39. Shaikh, N. *et al*. Pleomorphic xanthoastrocytoma: a brief review. *CNS Oncol.* **8**, CNS39 (2019).
40. Celiku, O., Johnson, S., Zhao, S., Camphausen, K. & Shankavaram, U. Visualizing molecular profiles of glioblastoma with GBM-BioDP. *PLoS One* **9**, e101239 (2014).
41. Deng, X. et al. Glioma-BioDP: database for visualization of molecular profiles to improve prognosis of brain cancer. *BMC Med. Genomics* **16**, 168 (2023).
42. Zhao, Z. et al. Chinese glioma genome atlas (CGGA): a comprehensive resource with functional genomic data from Chinese glioma patients. *Genomics Proteomics Bioinformatics* **19**, 1–12 (2021).
43. Zhang, C. et al. Epigenetic regulation of mRNA mediates the phenotypic plasticity of cancer cells during metastasis and therapeutic resistance (Review). *Oncol Rep.*https://doi.org/10.3892/or.2023.8687 (2024)
44. Yabo, YA. et al. Cancer cell heterogeneity and plasticity: a paradigm shift in glioblastoma. *Neuro Oncol.* **24**, 669–682 (2022)
45. Higa, N. et al. A tailored next-generation sequencing panel identified distinct subtypes of wildtype IDH and TERT promoter glioblastomas. *Cancer Sci.* **111**, 3902–3911 (2020).
46. Higa, N. *et al*. Prognostic impact of *PDGFRA* gain/amplification and *MGMT* promoter methylation status in patients with *IDH* wild-type glioblastoma. *Neurooncol. Adv.* **4**, vdac097 (2022).
47. Ogawa, K. et al. Giant cell glioblastoma is a distinctive subtype of glioma characterized by vulnerability to DNA damage. *Brain Tumor Pathol.* **37**, 5–13 (2020).
48. Tihan, T., Vohra, P., Berger, M. S. & Keles, G. E. Definition and diagnostic implications of gemistocytic astrocytomas: a pathological perspective. *J. Neurooncol.* **276**, 175–183 (2006).
49. R Foundation for Statistical Computing. R: a language and environment for statistical computing. https://www.r-project.org/ (2024).


## Acknowledgements

The authors greatly appreciate the excellent technical assistance provided by Ms. Yukari Nishida-Kirita and Ms. Emi Kubota at the Department of Pathology, Kagoshima University Hospital, and Ms. Tomoko Takajo at the Department of Neurosurgery, Kagoshima University Graduate School of Medical and Dental Sciences.

## Author contributions

MK: pathological examination, integrative diagnosis, and investigation. SY: gene methylation analysis and statistical analysis. TA: genomic analysis and annotation. NH: resources and supervision. HU: resources. HY: resources. KM: gene methylation analysis. JY: resources. KY: conceptualization, resources, and funding acquisition. RH: resources, and funding acquisition. AT: writing-original draft, review and editing, and funding acquisition.

## Competing interests

The authors declare that they have no competing interests.

## Ethics approval and consent to participate

The study was conducted in accordance with the principles of the Declaration of Helsinki. The study was approved by the Ethics Committee of Kagoshima University Hospital (approval number: 180104), and written informed consent was obtained from each patient.

## Additional information

**Supplementary Information** The online version contains supplementary material available at https://doi.org/10.1038/s41598-024-76826-8.

**Correspondence** and requests for materials should be addressed to R.H. or A.T.

**Reprints and permissions information** is available at www.nature.com/reprints.

**Publisher's note** Springer Nature remains neutral with regard to jurisdictional claims in published maps and institutional affiliations.